Climate Variability in the Andes of Ecuador and Its Relation to Tropical Pacific and Atlantic Sea Surface Temperature Anomalies

MATHIAS VUILLE, RAYMOND S. BRADLEY, AND FRANK KEIMIG

Climate System Research Center, Department of Geosciences, University of Massachusetts, Amherst, Massachusetts

ABSTRACT

The main spatiotemporal modes of seasonal precipitation and temperature variability in the Andes of Ecuador (1°N–4°S) and their relation to tropical Pacific and Atlantic sea surface temperature anomalies (SSTAs) between 1963–92 are identified based on rotated principal component analysis and cross-correlation techniques. Outgoing longwave radiation composites are analyzed during periods of strong oceanic forcing to confirm the proposed physical mechanisms. Despite the close proximity to the Pacific, precipitation variability in the Andes of Ecuador is not related to SSTA in the tropical Pacific domain alone. The El Niño–Southern Oscillation influence is most dominant in the northwestern part of the Andes during December–February (DJF) and in the eastern Cordillera during June–August (JJA) and in both cases associated with below- (above-) average precipitation during El Niño (La Niña) years. During most of the year precipitation variability over the eastern Andes is related to a dipolelike correlation structure in the tropical Atlantic, featuring positive correlations with SSTA to the south of the ITCZ and negative correlations to the north. The proposed mechanism involves positive SSTA in the tropical South Atlantic and contemporaneous negative SSTA in the tropical North Atlantic, resulting in increased rainfall over the eastern Cordillera. The only region with slightly increased precipitation during El Niño events is confined to a narrow area along the western Andean slope between 1° and 3°S in close proximity to the Pacific. However, this relationship is weak and only apparent in DJF. Temperature variability in the Andes can largely be explained by SSTA in the tropical Pacific domain. The temperature response closely follows SSTA in the Niño-3 and Niño-3.4 regions with approximately one-month lag. The northernmost part of the Andes (north of 0.5°N) is the only region where temperatures are significantly correlated with tropical North Atlantic SSTA.

1. Introduction

The anomalously heavy rainfall associated with El Niño is the dominant precipitation signal in coastal areas of northern Peru and Ecuador on interannual timescales (e.g., Horel and Cornejo-Garrido 1986; Goldberg et al. 1987; Tapley and Waylen 1990; Rossel 1997). Torrential rains, high river runoff, and flooding are the result of strong positive sea surface temperature anomalies (SSTA) along the coast of Peru and Ecuador and of an equatorward expansion and intensification of the intertropical convergence zone (ITCZ) over the eastern Pacific. On the other hand, a very strong and stable low-level inversion traps moisture in the surface layer during cold phases (La Niña) of the El Niño–Southern Oscillation phenomenon (ENSO). Little is known, however, concerning how far inland toward the Andes this signal is evident and dominant. Goldberg et al. (1987) reported

that in northern Peru the major impact of El Niño is limited to the coastal plains below 300 m, although at higher elevations a rainfall enhancement above average also seems to occur during El Niño events.

Due to the lack of sufficient information and because of the close proximity of the Andes to the Pacific Ocean, several studies have simply extrapolated the coastal ENSO signal into the Andean region. In reality however, the Andes have a very complex spatial precipitation pattern, influenced by both the Pacific and the Amazon basin, to the east of the Andes. While at higher levels, easterlies with varying meridional components prevail throughout the year, the Andes represent a powerful divide for the lower tropospheric flow. Accordingly, coastal areas and the lower western slopes of the Andes are influenced mainly by air masses originating in the Pacific, while the eastern part of the country is dominated by moisture-bearing easterly trade winds originating over the tropical Atlantic and Amazon basin (Hastenrath 1981). The inter-Andean valleys between the western Cordillera Occidental and the eastern Cordillera Oriental experience a varying influence from oceanic and continental air masses with two rainy seasons (February–May and October–November). The first

Corresponding author address: Dr. Mathias Vuille, Climate System Research Center, Department of Geosciences, University of Massachusetts, Morrill Science Center, Amherst, MA 01003-5820.
E-mail: mathias@geo.umass.edu
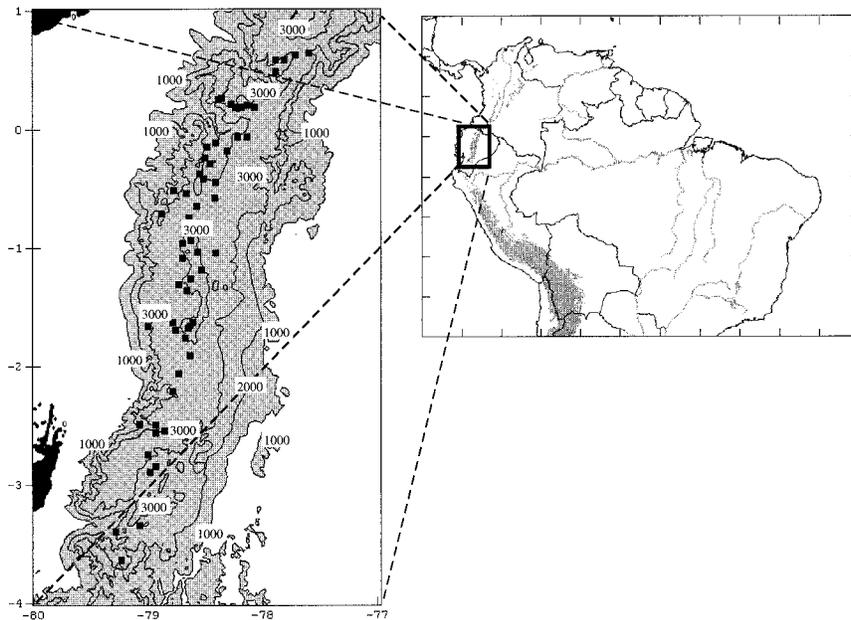
FIG. 1. Location of the stations with precipitation and temperature records in the Andes of Ecuador that were used in this study. Location of Ecuador is shown in the inset. Areas >1000 m are shaded.

dry period (June–September) is much more pronounced than the second one around December. As air masses lose much of their humidity on both flanks of the Andes, precipitation amounts in the inter-Andean valleys and basins are rather low, varying between 800 and 1500 mm yr^{-1}.

The aim of this study is to clarify the spatiotemporal relationship between tropical Pacific and Atlantic SSTA and precipitation and temperature variability in the Andes of Ecuador using a dense climate station network. This analysis is based on principal component analysis (PCA) of tropical Pacific and Atlantic SSTA, and precipitation and temperature anomalies between 1963–92 from a network of high-altitude stations (>2500 m) in the Andes of Ecuador.

In the next section we describe the data we used in this study and the methods that were applied. Section 3 presents a short summary of the results from the PCA on the tropical Pacific and Atlantic SST's. Section 4 presents the results of the PCA of precipitation separately for each 3-monthly season and includes a discussion on how these main modes relate to oceanic forcing. Results from outgoing longwave radiation (OLR) composite analysis during extreme warm and cold periods of the respective SST modes yield further evidence on the mechanisms involved. Section 5 presents the same results for temperature, however without seasonal subdivision. Section 6 presents a discussion of the results obtained in sections 3–5, summarizes this study, and ends with some concluding remarks.

2. Data and methods

Monthly mean SST data on a 1° lat × 1° long grid were obtained from the global sea-ice and sea surface temperature dataset, GISST version 2.3a (Hadley Center, Meteorological Office, Bracknell, United Kingdom). The original data was resampled into 2° × 2° grid cells, smoothed using a Hamming weights low-pass filter with a notch at $f = 4$ cycles yr^{-1}, thereby removing fluctuations with periods of less than 3 months (see Stearns and David 1988) and monthly anomalies were computed over the tropical Pacific (30°N–30°S, 160°E–80°W) and Atlantic (30°N–30°S, 80°W–10°E) by subtracting the mean monthly values for the period 1963–92.

Monthly National Oceanic and Atmospheric Administration (NOAA) interpolated OLR data with a 2.5° lat × 2.5° long grid was obtained from NOAA Climate Diagnostics Center for the period June 1974–December 1992, with some months in 1978 having missing data (see Liebmann and Smith 1996).

Monthly precipitation and monthly mean temperature data from stations between ~2500 and ~3700 m covering the entire Andean range of Ecuador from 1°N to 4°S was obtained from the Hydrology Department of the National Polytechnic Institute in Quito, Ecuador. Data after 1990 was obtained from the Instituto Nacional de Hidrología e Meteorología (INAMHI), Quito. From this original dataset of 214 precipitation and 78 temperature stations, a subset of 54 (26) precipitation (temperature) stations was selected, equally distributed along the Andean range (see Fig. 1) to avoid problems as-

sociated with computing principal components (PCs) for irregularly spaced data (Karl et al. 1982). The temperature network, unfortunately, is much less dense; however, it is considered sufficient, as temperature shows less spatial variability than precipitation. All selected stations had a record that was at least 90% complete in the time period analyzed, 1963–92. All data were error checked and, if necessary, homogenized using double-cumulative techniques. Cross correlations between all stations were computed and missing data periods were filled using linear regression with stations showing the highest correlation, always significant at the 99% level. The time period 1963–92 was selected because the installation of a dense station network in Ecuador began only in the early 1960s. Only a few very long records from Ecuador are available, insufficient for a thorough spatial analysis in the Andes. To account for noise in the record associated with individual months, and to capture modes of variability that can be attributed to a particular season, analysis of precipitation variability was carried out on the basis of 3-monthly sums. According to the seasonal distribution and the varying continental and Pacific influence on precipitation in the Andes, the year was subdivided into December–February (DJF) (minor dry period), March–May (MAM) (main rainy period), June–August (JJA) (main dry period), September–November (SON) (minor rainy season). All 3-monthly sums were transformed into γ probabilities, as precipitation data shows a distinctly asymmetric distribution, skewed to the right and bounded by 0. Temperature data were smoothed in the same way as the SST data and monthly anomalies were computed by subtracting the mean monthly values for the period 1963–92. Temperature analysis was performed on the entire continuous record without subdivision into seasons.

Next a rotated PCA was performed in the S-mode (spatial) sense based on the interstation correlation matrix of the precipitation and temperature data. Several tests were applied to determine the number of unrotated principal components (UPCs) that contain a nonrandom signal (North et al. 1982; Overland and Preisendorfer 1982). The UPCs retained were Varimax-rotated (VPCs) and their spatial loading patterns were plotted using spherical kriging to interpolate between the precipitation and temperature stations. Only the first unrotated principal component of temperature (T-UPC1) was retained for further analysis, because of the less representative precipitation delineation of UPCs (Richman and Lamb 1985). For precipitation the PCA was done separately for the 3-month periods DJF, MAM, JJA, and SON.

The resulting time series (factor scores) of the UPCs and VPCs were cross-correlated with tropical Pacific and Atlantic SSTA. For seasonal correlations (precipitation), the initial month of the corresponding season was used (e.g., DJF precipitation was correlated with December SSTA). For monthly correlations (temperature), both contemporaneous and time-lagged analysis

TABLE 1. Eigenvalues and percentage of total and cumulative explained variance for UPC1 and VPC1-5 based on the principal components analysis of tropical Pacific (PAC) and Atlantic (ATL) SSTA.

Principal component	Eigenvalue	Total explained variance (%)	Cumulative explained variance (%)
PAC-UPC1	65.82	35.39	—
ATL-UPC1	63.17	29.66	—
PAC-VPC1	45.20	24.30	24.30
PAC-VPC2	26.80	14.41	38.71
PAC-VPC3	15.31	8.23	46.94
PAC-VPC4	14.86	7.99	54.93
PAC-VPC5	14.29	7.68	62.61
ATL-VPC1	49.76	23.36	23.36
ATL-VPC2	39.32	18.46	41.82
ATL-VPC3	31.52	14.80	56.62
ATL-VPC4	18.56	8.71	65.33
ATL-VPC5	14.09	6.62	71.95

were carried out to account for a possible lag between oceanic forcing and temperature response in the Andes of Ecuador. All correlation significance levels account for serial correlation in the data by an adjustment in the degrees of freedom (see Davis 1976). Since such cross correlations of time series may lead to statistically significant, but physically meaningless results, we next performed the reversed procedure to confirm our findings. The PCs were extracted separately over the tropical Pacific (30°N–30°S, 160°E–80°W) and Atlantic (30°N–30°S, 80°W–10°E) from monthly SSTA in the same way as for the temperature data. Again only the first unrotated PC (PAC-UPC1, ATL-UPC1) was retained in the analysis together with the Varimax-rotated solutions (PAC-VPCs, ATL-VPCs). Their score time series were cross-correlated with the station data from the Ecuadorian Andes (3-monthly precipitation and monthly temperature data). Coherency maps of cross correlations between temperature or precipitation and oceanic forcing were plotted, again tested for significance, and the results of this second approach were compared to the patterns obtained previously from the first analysis to see whether they compared favorably.

Finally, seasonally averaged OLR composite difference patterns (warm–cold) over tropical South America were analyzed for extreme phases of the respective SSTA modes. Warm (W) and cold (C) phases were defined as periods when the standardized score time series of the respective SSTA mode is >1 (warm) and <−1 (cold) during the month of forcing (i.e., during December for the DJF composites) and are indicated in the score time series in Fig. 5.

3. Modes of tropical Pacific and Atlantic SST variability

Table 1 shows the basic statistics of the PCA performed on the SSTA in the Atlantic and Pacific. The first 5 PCs were considered to contain a nonrandom signal in both the Atlantic and Pacific analysis and there-
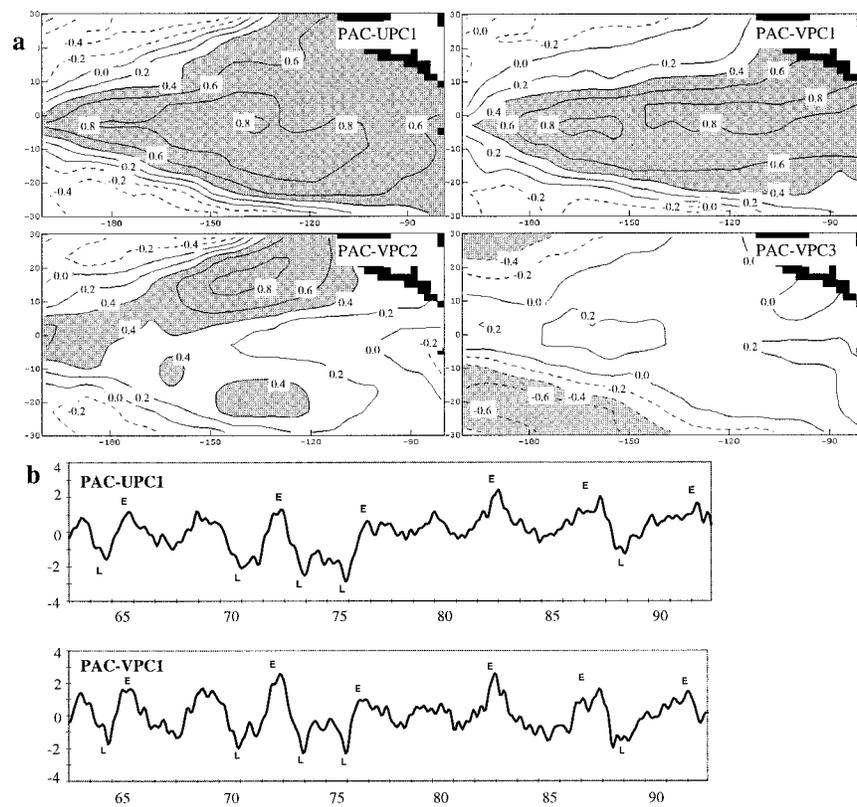
FIG. 2. (a) Loading pattern of tropical Pacific SSTA PAC-UPC1 and PAC-VPC1–3 with contour interval 0.2, values >0.40 or <−0.40 shaded, and negative contours dashed. (b) Score time series of PAC-UPC1 and PAC-VPC1 with E and L indicating El Niño (E) and La Niña (L) events.

fore retained and Varimax rotated. Only the modes that are of further relevance for this study are discussed below and shown in Figs. 2 and 3. A more detailed description of the tropical SSTA modes can be found in Vuille et al. (2000).

SST variability on interannual timescales in the tropical Pacific is largely controlled by the ENSO phenomenon. Both PAC-UPC1 and PAC-VPC1 are associated with a clear ENSO signal showing the typical characteristics in both their spatial pattern (Fig. 2a) as well as in their temporal evolution (Fig. 2b). The pattern is almost identical to the first Pacific EOF found by Enfield and Mayer (1997) and also strongly resembles the composite SSTA distribution for the mature phase of six historical El Niños found by Rasmusson and Carpenter (1982). The dominant mode of Pacific SSTA features the typical broad tongue centered on the equator and extending westward beyond the dateline. All major El Niño and La Niña periods in the time interval 1963–92 are represented as high- (El Niño) and low- (La Niña) score values in both time series (Fig. 2b). Further evidence comes from the correlation of Niño-3.4 (5°N–5°S, 170°–120°W) with PAC-UPC1 ($r = 0.91$, significant at 99.9% level) and of Niño-3 (5°N–5°S, 150°–90°W) with PAC-VPC1 ($r = 0.90$, significant at 99.9% level). Also evident in Fig. 2b is the major shift observed

in the climatic regime of the Pacific since the late 1970s, with a tendency toward more frequent El Niño and fewer La Niña events. PAC-VPC2 also contains an ENSO-related signal; however, most of the explained variance is located over the tropical North Pacific, while PAC-VPC3 is not primarily related to ENSO and explains most SSTA variability over the southwestern tropical Pacific.

The spatial loading patterns of ATL-UPC1 and ATL-VPC1–3 and the score time series of ATL-VPC1–2 are shown in Fig. 3. While ATL-UPC1 shows a pattern of strongest loadings in a band across the equatorial Atlantic extending from northeastern Brazil toward the coast of west Africa, ATL-VPC1 and ATL-VPC2 show a better resolved picture with most of the explained variance within the trade wind regions of the tropical North and South Atlantic, respectively. These two Varimax-rotated solutions are almost identical to EOF1 and EOF2 presented by Enfield and Mayer (1997), although the order between the first and second EOF is reversed in their analysis.

The domain of ATL-VPC1 is also the region where the ENSO influence on tropical Atlantic SST's is best developed. About 50%–80% of the anomalous SST variability in the area of the northeastern trades west of 40°W along 10°–20°N and extending into the Caribbean
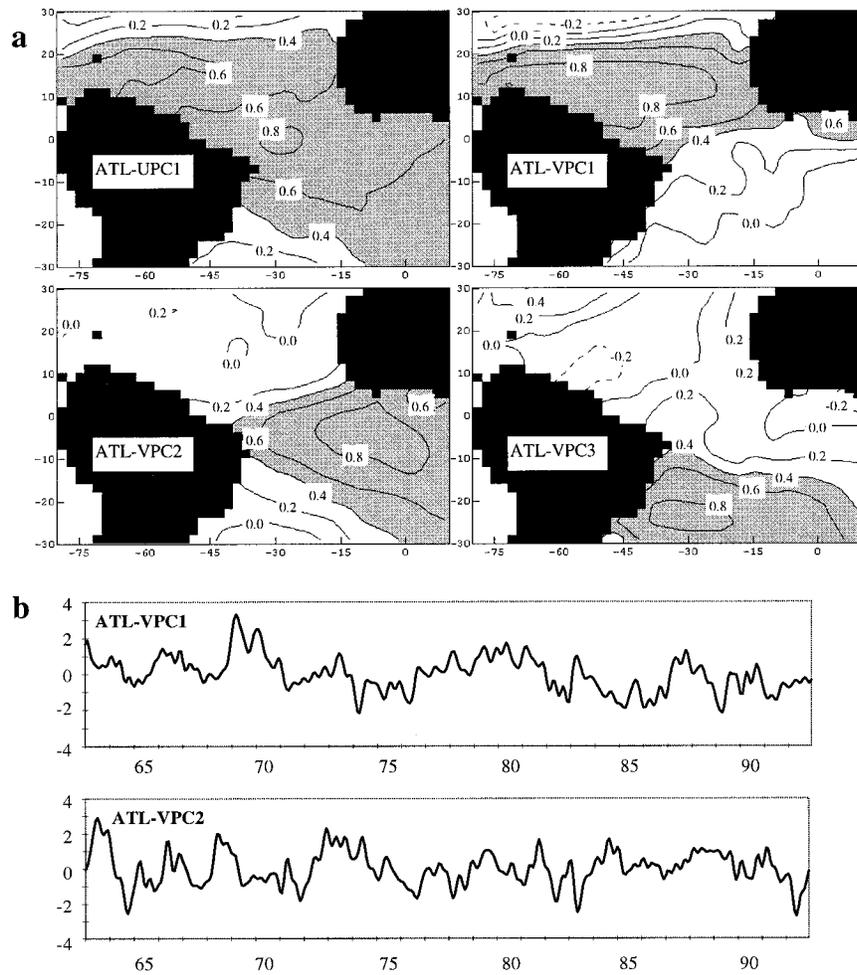
FIG. 3. (a) Same as Fig. 2a but for tropical Atlantic SSTA principal components (ATL-UPC1 and ATL-VPC1–3).(b) Same as Fig. 2b but for score time series of ATL-VPC1–2.

is related to ENSO, with Atlantic warmings occurring 4–5 months after the mature phase of Pacific warm events during boreal spring MAM (Enfield and Mayer 1997). These Atlantic warm events are important when considering precipitation anomalies over the tropical South American continent, because the trade winds of both hemispheres cross the isotherms toward the warmest water lying below the low-level confluence that defines one aspect of the ITCZ. Accordingly, the northeastern trades are normally strongest in February when the South Atlantic is warmest, and the southeastern trades are strongest in August when the North Atlantic is warmest. The ITCZ reaches its southernmost position close to the equator in March and its northern limit along 9°–10°N in August (Hastenrath and Heller 1977). During warm events in the tropical North Atlantic, which follow a Pacific ENSO, a significant relaxation of the northeastern trades can be observed, followed by a northward shift in the latitude of the ITCZ. Over the tropical South Atlantic, a strengthening of the subtropical high pressure system, including a reinforcement of

the associated southeastern trades occurs (Hameed et al. 1993; Enfield and Mayer 1997). These periods are intimately related to drought conditions over northeastern Brazil and the Amazon basin (e.g., Chung 1982; Mechoso et al. 1990; Uvo et al. 1998). However, opinions on the ENSO response in the tropical South Atlantic are controversial, ranging from a weak warming, especially off the coast of southern Brazil (Enfield and Mayer 1997), to no significant response (Uvo et al. 1998) or even a cooling. During the high phase of the SO (Pacific La Niña events), the response is broadly inverse, featuring unusually low SST's in the tropical North Atlantic, strengthened northeastern trade winds and the near-equatorial low pressure trough and embedded confluence zone displaced anomalously far to the south.

ATL-VPC2 is very similar to EOF1 found by Enfield and Mayer (1997) in their analysis for the entire tropical domain (30°N–30°S), but also to EOF1 of Venegas et al. (1996), for the South Atlantic domain. This mode represents a uniform in-phase SST response over the entire tropical South Atlantic, intimately related to the

TABLE 2. Eigenvalues and percentage of total and cumulative-explained variance of unrotated (UPC1) and Varimax-rotated principal components (VPCs) of seasonal precipitation (DJF, MAM, JJA, and SON) and monthly temperature anomalies (T-UPC1, TVPC1-4).

Principal component	Eigenvalue	Total explained variance (%)	Cumulative explained variance (%)
DJF-VPC1	19.91	36.88	36.88
DJF-VPC2	14.72	27.27	64.15
MAM-VPC1	11.18	20.70	20.70
MAM-VPC2	10.82	20.03	40.73
MAM-VPC3	10.08	18.67	59.40
JJA-VPC1	12.14	22.48	22.48
JJA-VPC2	11.56	21.40	43.88
JJA-VPC3	11.35	21.02	64.90
SON-VPC1	13.00	24.08	24.08
SON-VPC2	11.35	21.02	45.10
SON-VPC3	10.06	18.63	63.73
T-UPC1	10.24	39.37	—
T-VPC1	5.22	20.08	20.08
T-VPC2	4.83	18.57	38.65
T-VPC3	3.85	14.80	53.45
T-VPC4	2.60	9.99	63.44

strengthening and weakening of the subtropical anticyclone (Venegas et al. 1996). ATL-VPC3 resembles Venegas et al. (1996) EOF2 with the highest fraction of explained local variance in the southernmost part of the tropical South Atlantic. In addition, it exhibits a weak tendency toward a dipole structure with negative loadings in the tropical North Atlantic.

4. SSTA relation to precipitation

a. DJF

The basic statistics of the PCA of station precipitation data is given in Table 2 for all seasons. The analysis of DJF precipitation yielded only two eigenvectors with significant, nonrandom information for subsequent rotation and further analysis. Their spatial-loading patterns and score time series are shown in Figs. 4a, 4c, and 5a,b. DJF-VPC1 shows highest loadings in the northwestern Andes (Fig. 4a) and accounts for 36.9% of the total variance. This mode is clearly related to the ENSO phenomenon, all El Niño events except the anomalous 1982/83 event are associated with negative scores and all La Niña events feature above-average precipitation (Fig. 5a). Clearly El Niño events are associated with a decrease in DJF precipitation in the northwestern Ecuadorian mountains, that is, the coastal signal with increased precipitation and flooding is reversed toward the Andes. This strong ENSO signal in DJF precipitation can be explained partly by the fact that the Pacific influence is generally strongest during this season (Bendix and Lauer 1992) and partly because ENSO events often tend to peak around DJF. In addition, highly significant pixel-based cross correlations of the score time series with December SSTA emerge in the central tropical Pacific domain of PAC-UPC1 and PAC-

VPC1 (Fig. 6a), and to a smaller extent also over the northernmost part of the tropical Atlantic. When the December scores of the Pacific ENSO modes are correlated with DJF station precipitation data, a very similar pattern emerges. Figure 4b shows significant correlations between DJF precipitation and PAC-VPC 1 in the northwestern part of the Andes [a correlation 0.37 (0.47) is statistically significant at the 95% (99%) level]. The results suggest that DJF precipitation is indeed strongly governed by Pacific ENSO events; however, the affected area seems to be smaller than assumed from the previous analysis (Fig. 4a) and confined to the northwestern part of the Andes. Correlations with PAC-UPC1 (not shown) result in almost identical patterns. Figure 7a shows the difference in OLR during DJF for periods with warm (El Niño) and cold (La Niña) SSTA, based on the December scores of PAC-UPC1. Clearly E1 Niño (La Niña) periods are associated with a substantial increase (decrease) in OLR, centered over the tropical North Atlantic and the northeastern part of tropical South America. A similar pattern has been presented by Kousky and Kayano (1994) as the principal OLR mode related to the Southern Oscillation. Noteworthy is also the secondary OLR maximum that emerges over northwestern South America. Although the resolution of the OLR data is insufficient to resolve the spatial variability over Ecuador, the large-scale pattern suggests that northernmost Ecuador is affected by the same mechanism that leads to increased aridity during El Niño in Columbia (see Hastenrath 1990; Poveda and Mesa 1997).

DJF-VPC2 explains most of the precipitation variability near the western slopes between 1° and 3°S (Fig. 4c). The correlation with SSTA (Fig. 6b) also suggests a relation to SST variability in the Pacific domain. However, correlations are lower than for DJF-VPC1 and their significance is confined to a much smaller area in the eastern tropical Pacific. The score time series of DJF-VPC2 (Fig. 5b) implies a rather weak relation with ENSO; only the very unusual 1982/83 event was associated with significantly increased precipitation in this area. Nevertheless, the precipitation response to ENSO on the western slope near 1°–3°S is of the same sign as in the coastal lowlands with El Niño years yielding generally higher precipitation than La Niña years (except for above-average precipitation during 1988/89). It seems that with respect to DJF precipitation this region tends to show a transitional ENSO behavior between the lowlands of Ecuador experiencing abundant rainfall during El Niño and the northwestern part of the Andes experiencing drought. However, as shown in Fig. 5b, the major dry years in the west-central Ecuadorian Andes, 1967/68, 1977/78, and 1984/85 are neither related to La Niña nor to El Niño and the highest precipitation was received during an El Niño (1982/83), a La Niña (1988/89), and a ''normal'' (1969/70) year. Also none of the Pacific ENSO modes (PAC-UPC1 and PAC-VPC1) yielded significant correlations with DJF station
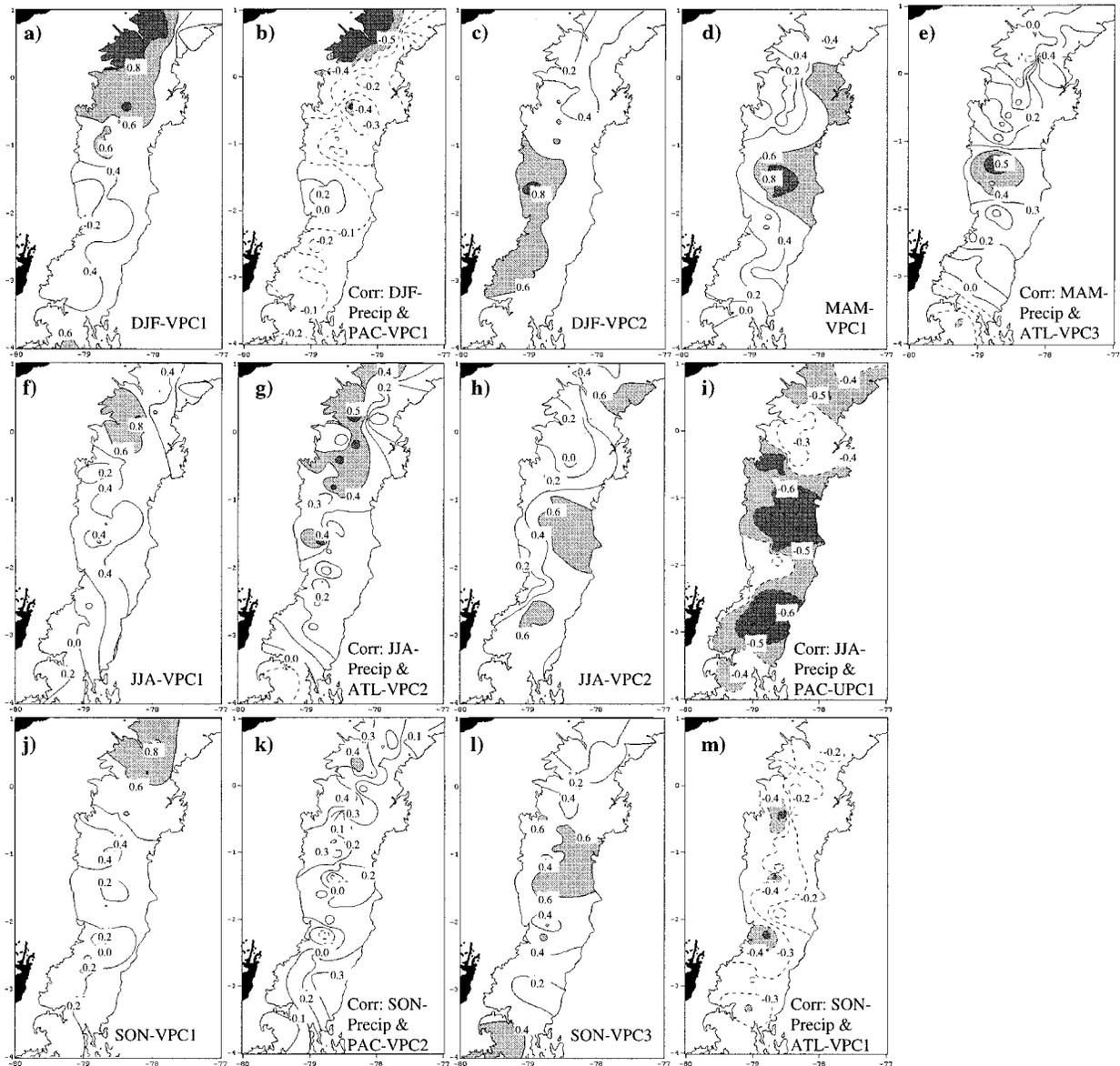
FIG. 4. (a) Loading pattern of DJF-VPC1 with contour interval 0.2, values >0.6 (0.8) shaded in light (dark) gray, and negative contours dashed. (b) Correlation pattern of DJF precipitation with Dec score of PAC-VPC1 with contour intervals of 0.1, negative contours dashed, and correlation coefficients >0.4 and <−0.4 (significant at 95% level) shaded in light gray and >0.5 and <−0.5 (significant at 99% level) shaded in dark gray.(c) Same as (a) but for DJF-VPC2. (d) Same as (a) but for MAM-VPC1. (e) Same as (b) but correlation between MAM precipitation and Mar score of ATL-VPC3. (f) Same as (a) but for JJA-VPC1. (g) Same as (b) but for correlation between JJA precipitation and Jun score of ATL-VPC2. (h) Same as (a) but for JJA-VPC2. (i) Same as (b) but for correlation between JJA precipitation and Jun score of PAC-UPC1. (j) Same as (a) but for SON-VPC1. (k) Same as (b) but for correlation between SON precipitation and Sep score of PAC-VPC2. (l) Same as (a) but for SON-VPC3. (m) Same as (b) but for correlation between SON precipitation and Sep score of ATL-VPC1. In all figures only data from areas >1500 m are plotted (delimited by contour lines).

precipitation in the region where the DJF-VPC2 mode is dominant (see Fig. 4b).

b. MAM

Three UPCs of MAM precipitation emerged after inspection of their eigenvalues as bearing significant nonrandom information and were thereafter rotated us-

ing the Varimax criterion (MAM-VPC1–3). However, only one of them, MAM-VPC1, showed a close association with tropical SSTA. This mode, explaining 20.7% of the total variance, is associated with a trend toward significantly increased precipitation over the three decades analyzed (Fig. 5c) and shows strongest loadings in the central-eastern part of the Andes between 0° and 2°S (Fig. 5d). Two main regions of sig-
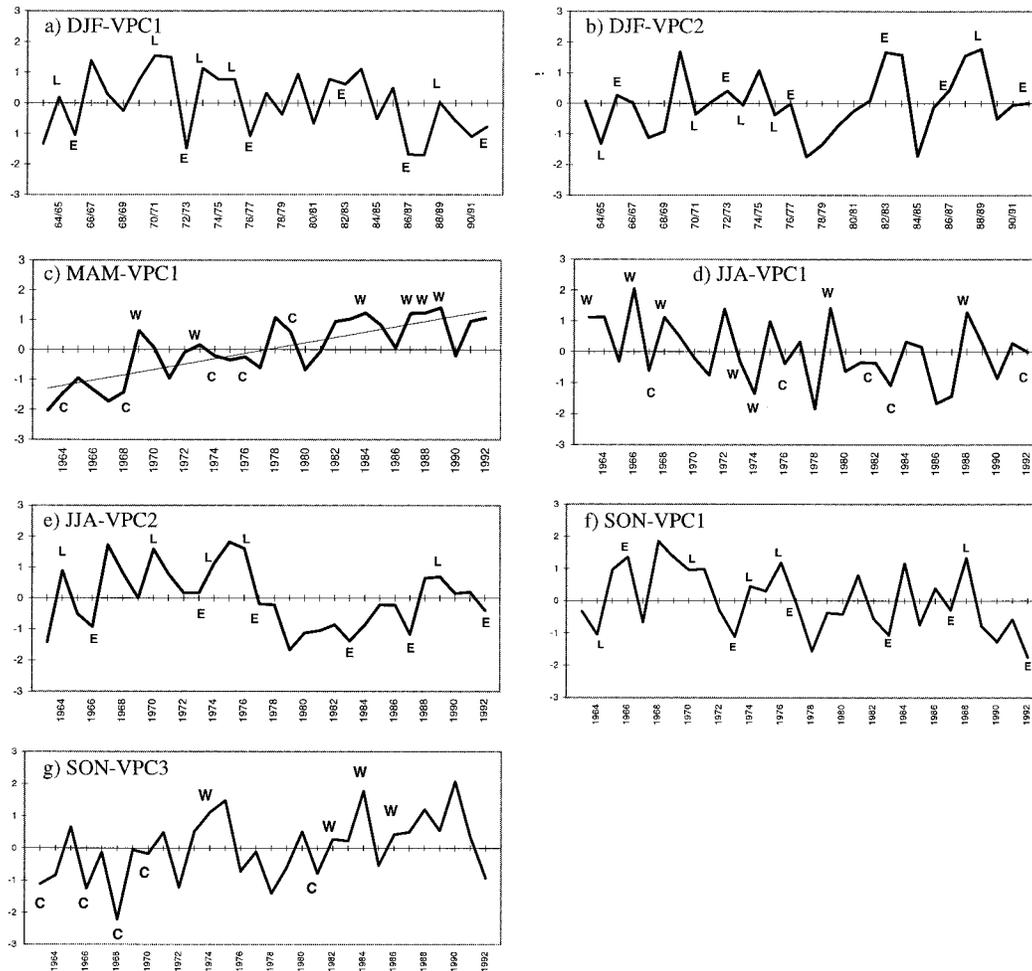
FIG. 5. (a) Score time series of DJF-VPC1 with E and L indicating El Niño (E) and La Niña (L) events. (b) Same as (a) but for DJF-VPC2. (c) Same as (a) but for MAM-VPC1 and with W and C indicating warm (W) and cold (C) Mar SSTA in the ATL-VPC3 domain (for explanation see text). (d) Same as (a) but for JJA-VPC1 and with C and W indicating cold (C) and warm (W) Jun SSTA in the ATLVPC2 domain. (e) Same as (a) but for JJA-VPC2. (f) Same as (a) but for SON-VPC1. (g) Same as (a) but for SON-VPC3 with W and C indicating periods when difference in Sep SSTA between ATL-VPC3 and ATL-VPC1 >1 (W) and <−1 (C) (for explanation see text).

nificant correlations with March SSTA emerged: one in the tropical South Pacific and a dipolelike structure in the Atlantic with negative correlations in the north off the coast of northeastern South America and positive correlations south of the equator (Fig. 6c). Although the area of significant correlations in the Pacific is substantial, the relation with MAM-VPC1 could not be confirmed by the reverse analysis. Neither PAC-UPC1 nor PAC-VPC1 show significant correlations with MAM station precipitation (not shown). Also, the fact that loadings are highest over the eastern part of the Andes is a hint toward a continental or even tropical Atlantic influence on MAM-VPC1 rather than a direct Pacific control. The dipolelike correlation structure in the Atlantic suggests increased precipitation over the eastern Cordillera when surface waters to the north are anomalously cold and warmer than normal to the south.

This behavior is best represented by ATL-VPC1 and ATL-VPC3 (see Fig. 3a); accordingly, March scores of both these modes were correlated with MAM station data. The results for ATL-VPC3 (Fig. 4e) and ATL-VPC1 (not shown) correspond quite well with the spatial loading pattern of MAM-VPC1 in Fig. 4d. Also the score time series of MAM-VPC1 (Fig. 5c) shows that above- (below-) average precipitation in MAM seems to be closely related to anomalously warm (cold) SSTs in the southern tropical Atlantic (ATL-VPC3 domain). Such conditions lead to convergence at low levels, a weakening of the South Atlantic subtropical anticyclone, a southward movement of the ITCZ, increased moisture advection toward the continent and increased precipitation in northeastern Brazil and the Amazon basin (e.g., Mechoso et al. 1990; Marengo 1992; Marengo and Hastenrath 1993; Wagner 1996).
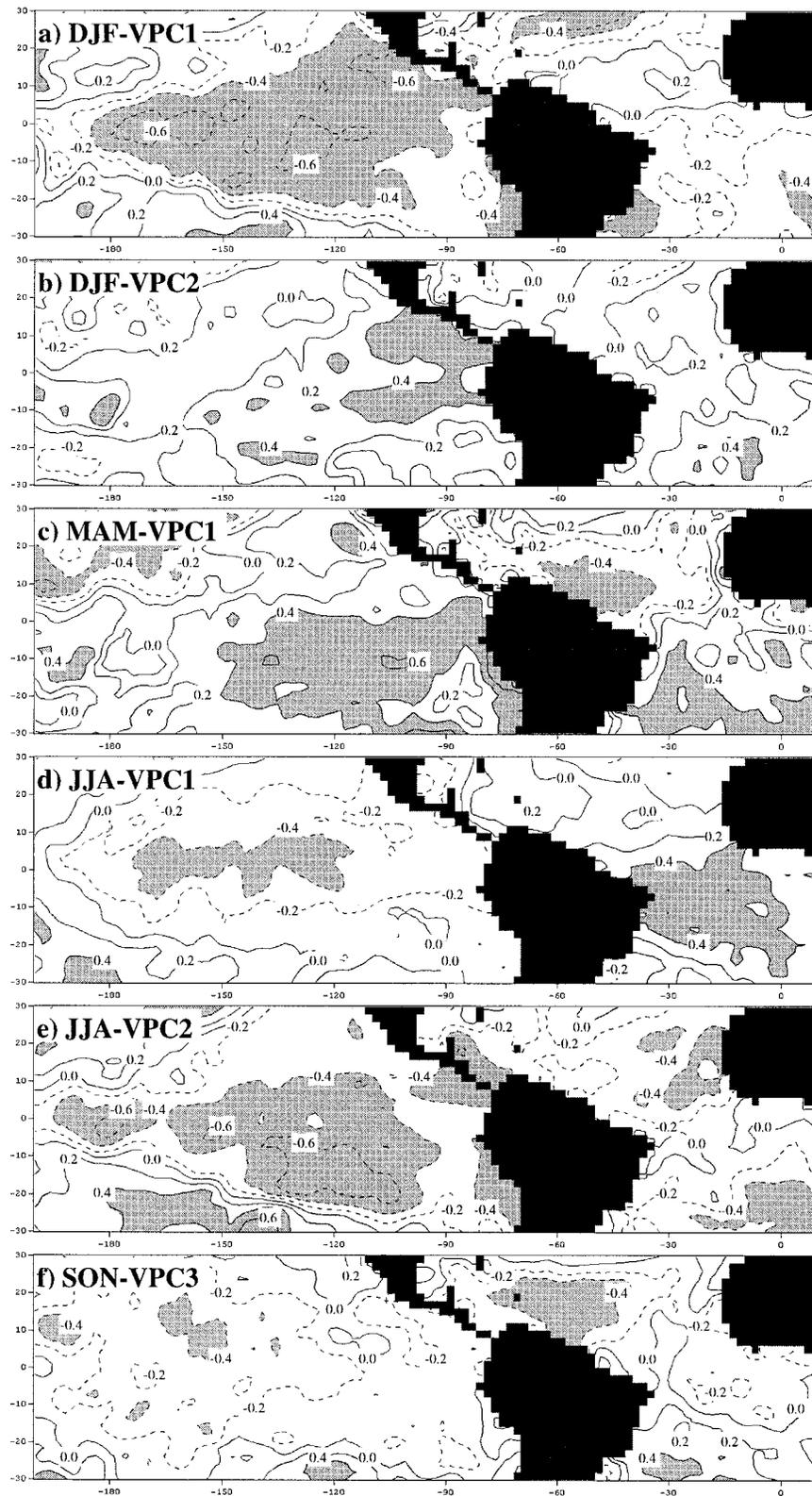
FIG. 6. (a) Pixel-based correlation of tropical Pacific and Atlantic SSTA in Dec with score time series of DJF-VPC1. Contour interval is 0.2; negative contours are dashed, and values <-0.4 and >0.4 (significant at 95% level) are shaded. (b) Same as (a) but for DJF-VPC2. (c) Same as (a) but for MAM-VPC1 correlation with Mar SSTA. (d) Same as (a) but for JJA-VPC1 correlation with Jun SSTA. (e) Same as (d) but for JJA-VPC2. (f) Same as (a) but for SON-VPC3 correlation with Sep SSTA.
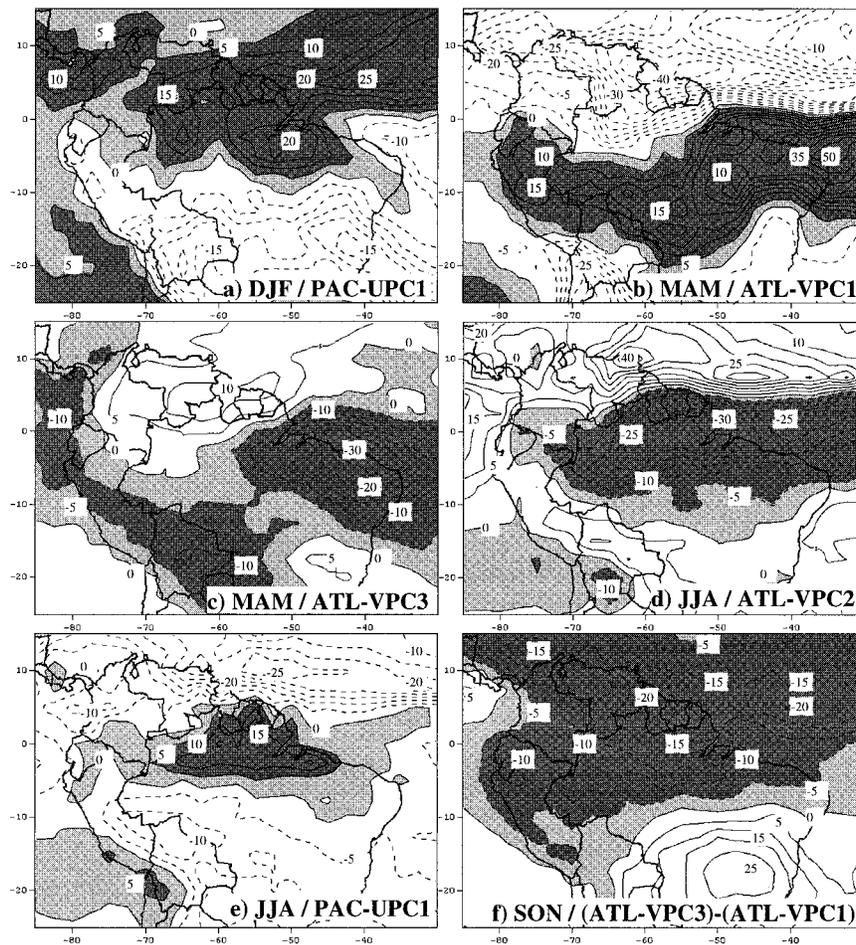
FIG. 7. (a) OLR difference composite for DJF between warm and cold periods based on Dec scores time series of PAC-UPC1. Contour interval is 5 W m^{-2}, negative contours are dashed, and positive values are shaded in light gray, values >5 W m^{-2} are shaded in dark gray.(b) Same as (a) but for MAM and based on difference between warm (W) and cold (C) periods in Mar scores of ATL-VPC1. (c) Same as (a) but for MAM and based on difference between warm (W) and cold (C) periods in Mar scores of ATL-VPC3 and with negative values shaded. (d) Same as (a) but for JJA and based on difference between warm (W) and cold (C) periods in Jun score time series of ATL-VPC2 (see Fig. 5d) and negative values shaded. (e) Same as (a) but for JJA and based on difference between El Niño (E) and La Niña (L) periods in Jun scores of PAC-UPC1 (see Fig. 5e). (f) Same as (a) but for SON and based on difference between events with large-positive (W) and large-negative (C) difference in Sep SSTA between ATL-VPC3 and ATL-VPC1 (see Fig. 5g) and with negative values shaded.

On the other hand, negative rainfall anomalies to the south of the equator during MAM are related to a strengthened South Atlantic trade flow, cold SSTA in the South Atlantic, and an early withdrawal of the ITCZ toward the warm SSTA over the tropical North Atlantic (e.g., Chung 1982; Nobre and Shukla 1996). The fact that these precipitation anomalies linked to anomalous ITCZ displacements are basinwide, is evident in the composite analysis presented in Figs. 7b,c. The shown MAM OLR patterns are based on the difference between warm and cold periods in the March scores of ATL-VPC1 (Fig. 7b) and ATL-VPC3 (Fig. 7c). A band of increased (decreased) OLR is associated

with a warm tropical North (South) Atlantic, extending from the tropical Atlantic south of the equator across southern tropical South America toward the southern tropical Andes, suggesting that even the eastern Cordillera of Ecuador is affected by the same process. Accordingly, the increase in precipitation in this part of the Andes over the last 30 years might be attributed to the observed increase in SSTs in the South Atlantic (Servain 1991). Although this relationship is somewhat speculative, the trend toward increased precipitation over the eastern Andes in MAM precipitation is consistent with results presented by Chu et al. (1994) reporting a significant negative OLR trend in western

Amazonia and along the eastern Cordillera, implying an increase of convection with time between 1974 and 1990.

c. JJA

JJA represents the driest season in Ecuador, but precipitation can still be substantial at times. Again three modes of precipitation variability emerged from the PCA as bearing significant, nonrandom information, but only the first two show potential relationships with tropical SSTA. Their spatial loadings are shown in Figs. 4f and 4h, the corresponding score time series in Figs. 5d,e and the correlations with pixel-based SSTA and OLR composites in Figs. 6d,e and 7d,e.

JJA-VPC1, explaining 22.5% of the total variance represents variability in the northwestern part of the study area and along the eastern part of the Andes (Fig. 4f) and is significantly correlated with a zone of contemporaneous negative SSTA in the central equatorial Pacific and positive SSTA in the equatorial Atlantic, south of the ITCZ (Fig. 6d). The relationship with the tropical South Atlantic again suggests an increase in precipitation associated with warm SSTA south of the ITCZ, similar to MAM-VPC1. The correlation of the dominant mode of SST variability in this part of the Atlantic, ATL-VPC2 (see Fig. 3a), with JJA station precipitation data, yielded a remarkably coherent pattern that matches well with its counterpart with significant correlations (at the 95% level) in the northwestern part of the Andes (compare Figs. 4f and 4g). The negative relationship with SSTA in the Pacific, however, implied in Fig. 6d, is much more pronounced in relationship with JJA-VPC2 (see Fig. 6e). In addition, the time evolution of JJA-VPC1 (Fig. 5d) does not support the notion of a possible ENSO relationship and is clearly related to SSTA forcing in the ATL-VPC2 domain. All cold events in this part of the tropical South Atlantic are associated with below-average precipitation, while all warm events (except for 1973 and 1974) include above-average precipitation. Further evidence is presented by the JJA OLR composite (Fig. 7d), based on the difference between warm and cold events in the ATL-VPC2 domain. It reveals a broad band of increased (decreased) convection associated with warm (cold) SSTA extending from the equatorial Atlantic across the Amazon basin toward the Andes of Ecuador.

JJA-VPC2 explains 21.4% of the total variance and is the dominant mode over most of the eastern range of the Andes (Fig. 4h). The score time series of JJA-VPC2 (Fig. 5e) and the SSTA correlation pattern (Fig. 6e), both suggest a strong and coherent ENSO influence. The score time series of JJA-VPC2 shows that all El Niño periods between 1963–92, except for the 1972/73 event, were associated with below-average precipitation during JJA, while all La Niña periods featured above-average precipitation. In addition, there seems to be a decadal-scale variability superimposed on the ENSO variability.

From the mid-1960s to the late 1970s all JJA seasons exhibit above-average precipitation, while the JJA dry season was more pronounced during the late 1970s and the 1980s (Fig. 5e). Figure 4i shows the correlation pattern of JJA station precipitation with PAC-UPC1 in June. The similarity with Fig. 4h is striking and corroborates the evident negative correlation between tropical Pacific SSTA and JJA precipitation. Further evidence comes from the OLR composite (OLR difference in JJA between El Niño and La Niña events) in Fig. 7e. The positive OLR anomalies, indicative of reduced (increased) convection during El Niño (La Niña) events are most pronounced in northern Brazil, but extend westward to the Andean foothills of Ecuador and northern Peru.

d. SON

SON represents the minor rainy season, associated with the southward passage of the ITCZ. This season also emerged as bearing three main modes of precipitation variability; however, only the first and the third mode are related to a possible tropical SSTA influence. Their spatial loading patterns are shown in Figs. 4j and 4l, the associated score time series in Figs. 5f,g and the correlation pattern with pixel-based SSTA and the OLR composite in Figs. 6f and 7f (for SON-VPC3 only).

SON-VPC1 explains 24.1% of the total variance and is a mode that is important only in the northern half of the country (Fig. 4j). The time evolution of SON-VPC1 (Fig. 5f) shows that, except for 1966, all Pacific warm events were associated with below-average SON precipitation, while all cold events, except for 1964, featured above-average SON precipitation. Again the same region in the northwestern part of the Andes seems to be sensitive to the ENSO phenomenon that already emerged as bearing an ENSO-related precipitation signal in the analysis of DJF (Fig. 4b) and JJA (Fig. 4i). Interestingly enough however, no significant correlations with Pacific SSTA occur, except for a small area in the northernmost part of the central tropical Pacific in the PAC-VPC2 domain (not shown). Figure 4k shows the correlation pattern between SON station precipitation and PAC-VPC2. Although the region of significant correlation is much smaller and not as coherent as suggested by Fig. 4j, an influence of the ENSO phenomenon on the northernmost part of the Andes is very likely.

The loading pattern of SON-VPC3 (Fig. 4l), which explains 18.6% of the total variance shows some resemblance to the one from MAM-VPC1 (Fig. 4d). This mode explains most of the SON precipitation variability in the central part of the study area, near 0.5–1.5°S, and to some extent also in the southernmost part of the Ecuadorian Andes. The correlation with SSTA yielded a coherent pattern of positive correlations with the tropical South Atlantic and negative correlations with the tropical North Atlantic off the coast of northeastern South America (Fig. 6f), similar to the one obtained for MAM-

VPC1 (Fig. 6c). Again this correlation structure in the Atlantic suggests increased precipitation when surface waters to the north are anomalously cold and warmer than normal to the south. ATL-VPC1 and ATL-VPC3 to some extent both represent this behavior and were therefore correlated with SON station precipitation. Figure 4m shows the result for ATL-VPC1, confirming a significant correlation between increased SON precipitation in the interior central part of the Andes (0°–2.5°S) and warm (cold) anomalies in the tropical South (North) Atlantic. The correlation pattern itself, however, does not bear much resemblance with the loading pattern of SON-VPC3 presented in Fig. 4l. The OLR composite (Fig. 7f), based on the difference between periods with a large-positive and a large-negative interhemispheric SSTA gradient (ATL-VPC3 − ATL-VPC1), suggest that entire northern tropical South America receives more SON precipitation when this SSTA gradient is large. Although no spatial variations can be deduced from the OLR analysis over the Andes, it provides clear evidence for the relationship between SON precipitation variability and the interhemispheric tropical Atlantic SSTA gradient. Further evidence stems from the score time series of SON-VPC3 (see Fig. 5g). While all Septembers featuring large-positive SSTA gradients (W: ATL-VPC3 − ATL-VPC1 > 1), yielded above-average SON precipitation, the contrary is the case for SON periods when September SSTA gradients where negative (C: ATL-VPC3 − ATL-VPC1 < −1).

5. SSTA relation to air temperature

The seasonal cycle of air temperature in Ecuador is negligible, accordingly the PCA of temperature is based on the entire calendar year using monthly temperature anomalies. The basic statistics of the PCA are given in Table 2. The first 4 unrotated PCs were identified as describing significant, non-random temperature variability and were subsequently rotated using the Varimax criterion (T-VPC1–4). However, only T-UPC1, T-VPC1, and T-VPC4 show variability that is clearly related to tropical SSTA. Their spatial-loading patterns are shown in Figs. 8a–c, their score time series in Figs. 9a–c and their correlation with tropical SSTA in Figs. 9d–f.

T-UPC1 (Fig. 8a) explaining 39.4% total variance, and T-VPC1 (Figure 8b) explaining 20.1% total variance, are clearly related to ENSO as can be seen both from their time evolution (Figs. 9a,b) and the correlation with tropical SSTA (Figs. 9d,e). T-UPC1 shows a clear pattern of significant correlations (99% level) over the entire equatorial Pacific during the preceding month (i.e., SSTA leads the temperature response by one month), extending from the coast of South America westward beyond the dateline (Fig. 9d). Highest correlations (significant at 99% level) are achieved with one-month lag between T-UPC1 and Niño-3.4 ($r =$ 0.79) and between T-VPC1 and Niño-3 ($r = 0.64$). Cor-

relations with the Southern Oscillation index (SOI) known to be negatively correlated with temperature anomalies in the Ecuadorian Andes (Aceituno 1988) and the coast of Ecuador (Halpert and Ropelewski 1992) yielded a less significant result [$r = -0.73$ (-0.55) for T-UPC1 (T-VPC1) when one month lag]. The spatial-loading patterns for T-UPC1 (Fig. 8a) and T-VPC1 (Fig. 8b) both imply that temperature anomalies associated with the ENSO phenomenon are reflected in a much stronger way in the western than in the eastern Cordillera. The reverse procedure, correlating PAC-UPC1 and PAC-VPC1 with temperature station data confirms this result, yielding correlation patterns (Figs. 8d,e) that are absolutely coherent with their counterparts in Figs. 8a,b.

The only region that shows little temperature sensitivity toward ENSO is the northernmost part of the Andes to the north of the equator. It is dominated by temperature mode T-VPC4 (Fig. 8c), obviously related to SST variability in the tropical North Atlantic (Fig. 9f), which, of course, in turn is again related to Pacific SSTA (see Enfield and Mayer 1997). The correlation with the dominant mode in the tropical North Atlantic (ATL-VPC1) is rather poor ($r = 0.45$) but nonetheless significant at the 95% level (Fig. 9c). If only SSTA in the Caribbean region are considered the correlation improves to 0.55, significant at 99% level. Figure 8f shows the correlation pattern between ATL-VPC1 and temperature station data, clearly reproducing the pattern in Fig. 8c.

6. Discussion and summary

The leading modes of seasonal precipitation and temperature variability in the Andes of Ecuador were identified by means of a PCA and their score time series correlated with tropical Pacific and Atlantic SSTA. As a result main regions of oceanic forcing, potentially related to climatic variability in the Andes of Ecuador, emerged. To confirm these results, a second PCA was applied to the SSTA data and the main modes of tropical Pacific and Atlantic SST variability extracted. Next the score time series of these main SSTA modes were correlated against station precipitation and temperature data to see whether similar patterns emerged. In most cases, this two-way approach strengthened our results. Some mismatches however highlight the importance of confirming the obtained results by applying an additional, independent analysis. Moreover the composite analysis of OLR data over tropical South America during periods of strong oceanic forcing helped to confirm some of the proposed physical mechanisms.

One of the most significant results of this study is the strong relationship between precipitation and the ENSO phenomenon in the northwestern part of the Andes. El Niño years are associated with below-average precipitation, while the opposite is true during La Niña events. The signal is strongest during the peak phase of ENSO (DJF) but also apparent during JJA and SON. These
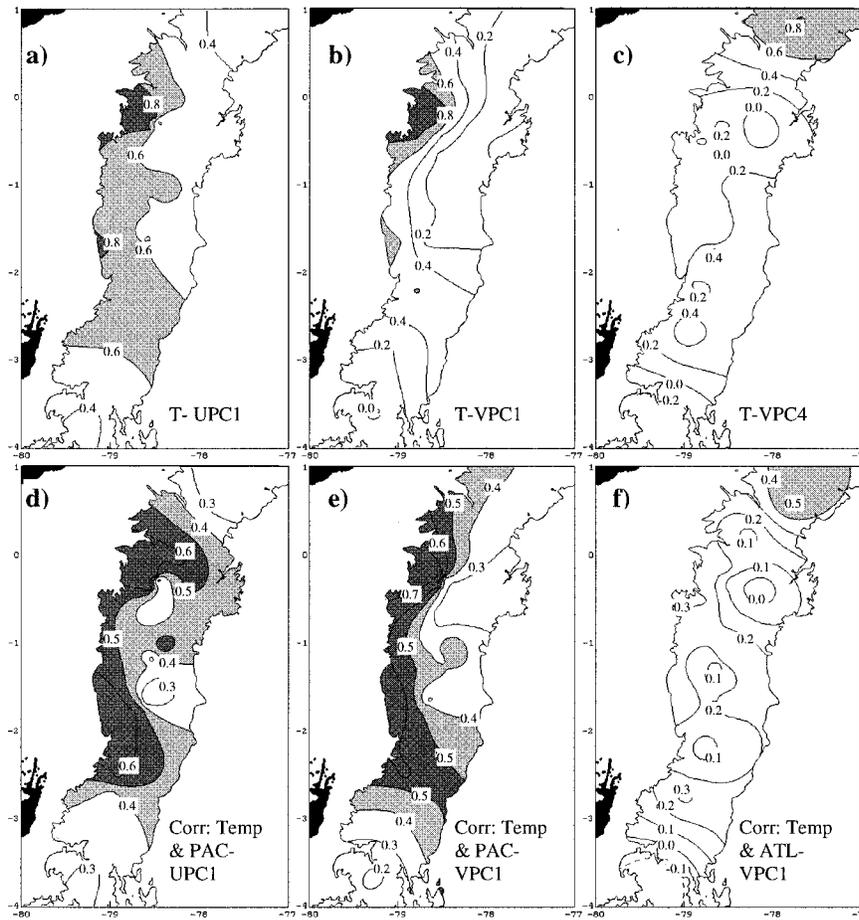
FIG. 8. Same as Fig. 4 but for air temperature. (a) Loading pattern of T-UPC1. (b) Same as (a) but for T-VPC1. (c) Same as (a) but for T-VPC4. (d) Correlation pattern of air temperature anomalies with PAC-UPC1 (one-month lag). (e) Same as (d) but correlation between air temperature anomalies and PAC-VPC1 (no lag). (f) Same as (d) but for correlation between air temperature anomalies and ATL-VPC1 (no lag).

results are consistent with observations made by Aceituno (1988), Hastenrath (1990), and Poveda and Mesa (1997) analyzing precipitation and river discharge in Columbia where the high phase of the Southern Oscillation (SO) (La Niña) is also associated with increased precipitation. Hastenrath (1990) relates this positive precipitation anomaly to a northward displaced ITCZ, weakened easterly trade winds over the Caribbean, and accelerated southwesterly cross-equatorial flow in the eastern Pacific. During El Niño periods on the other hand, an anomalous Hadley cell subdues and inhibits convection and precipitation in tropical South America during DJF (Poveda and Mesa 1997). This is consistent with our results, but it is suggested that the area influenced by these ENSO-related anomalies extends even as far south as northern Ecuador.

The eastern Cordillera is another region that shows similar negative precipitation anomalies associated with El Niño events; most prominently during the dry season (JJA). The eastern Andean range is not directly connected to a Pacific forcing but affected through atmospheric circulation anomalies over the interior of the continent. Kayano et al. (1988) and Kousky and Kayano (1994) showed that positive OLR anomalies and anomalous upper-air westerlies extend over the Central Andes, the Amazon basin, and the equatorial Atlantic during negative SO phases and that entire tropical South America is under the influence of the descending motion of an anomalous equatorial circulation inhibiting convective activity and reducing precipitation. This is consistent with the evidence presented here based on OLR composite analyses. During most of the year, however, the eastern Andes are more closely related to SSTA in the tropical Atlantic than the Pacific. Increased precipitation is associated with a dipolelike correlation structure in the tropical Atlantic featuring warmer than normal waters to the south of the ITCZ, while below-average SSTs occur to the north. This pattern is most effective when it occurs during boreal spring (MAM), but affects precipitation variability in the eastern Andes dur-
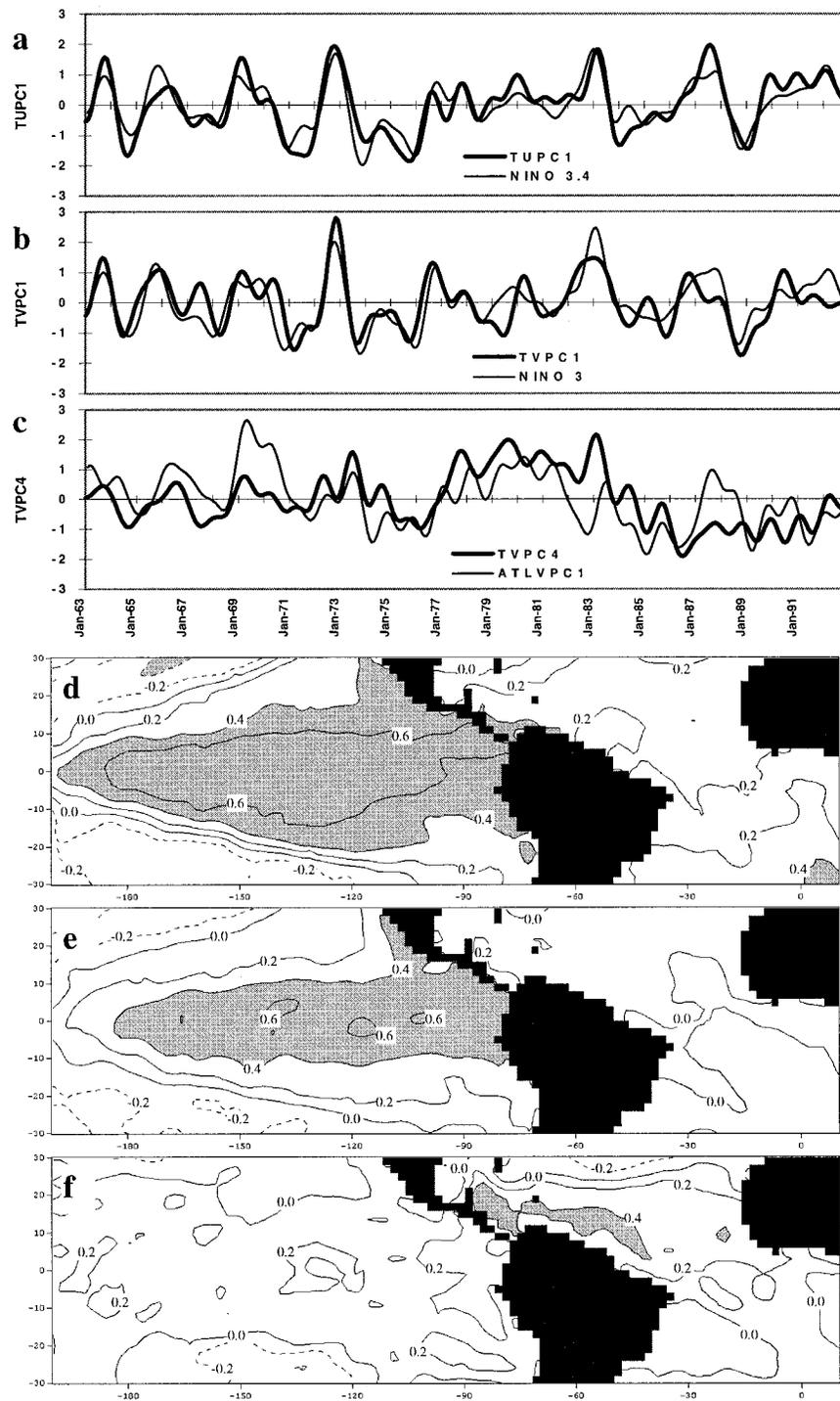
Fig. 9. (a) Score time series of T-UPC1 and Niño-3.4. (b) Score time series of T-VPC1 and Niño-3. (c) Score time series of T-VPC4 and ATL-VPC1. All time series have been low-pass filtered, retaining frequencies <1 cycle yr⁻¹. All SST time series lead air temperature PCs by one month. (d) Same as Fig. 6a but for T-UPC1 (one-month lag). (e) Same as (d) but for T-VPC1 (one-month lag). (f) Same as (d) but for T-VPC4 (no lag).

ing MAM, JJA, and SON. The warmer than normal conditions in the tropical South Atlantic result in a southward movement of the ITCZ and have been linked to enhanced moisture advection and increased precipitation over northeastern Brazil and the southern Amazon basin (e.g., Mechoso et al. 1990; Marengo 1992; Marengo and Hastenrath 1993; Wagner 1996). On the other hand, a strengthened South Atlantic trade flow, cold SSTA in the South Atlantic, and an early withdrawal of the ITCZ toward the warm SSTA over the tropical North Atlantic are associated with below-average precipitation in this region (e.g., Chung 1982; Nobre and Shukla 1996). The results presented here suggest that the influence of this tropical Atlantic SSTA mode and coupled ITCZ displacements upon precipitation anomalies extends even as far west as the eastern Andes of Ecuador. The Pacific influence on this mode, however, cannot be completely ruled out, since Pacific El Niño events trigger tropical North Atlantic warm events and thereby could lead to a reduction in Andean precipitation.

The western Andean slope between $1°–3°$S is the only region that shows a somewhat similar behavior to the coastal lowlands with respect to ENSO during its peak phase DJF. The close proximity of this region to the Pacific and the exposure of its slopes to air masses penetrating from the ocean may explain why the increased precipitation associated with El Niño, otherwise limited to lower coastal areas, can sometimes be observed in this part of the Andes. Similar observations have been made in coastal areas of northern Peru by Goldberg et al. (1987). The relationship however is weak and does not hold true during all ENSO events.

Temperature variability in the Andes of Ecuador closely follows SSTA in the tropical Pacific with a response time of approximately one month. Accordingly, the Pacific ENSO mode is the dominant mode associated with temperature anomalies in most parts of Ecuador except for the northernmost part of the country, north of $0.5°$N, which is more closely related to SSTA in the tropical North Atlantic domain. The rest of the Andes, however, is obviously very directly affected by SST changes in the tropical Pacific. Interestingly, temperature anomalies in the Andes closely follow SSTA in the central equatorial Pacific (Niño-3 and Niño-3.4 regions). This is in contrast to the lowlands of Ecuador that are more closely related to SSTA in the Niño-1 and Niño-2 regions off the coast (Rossel 1997). The loading patterns of the leading temperature modes (T-UPC1 and T-VPC1) and the correlation pattern of PAC-UPC1 and PAC-VPC1 with station temperature anomalies both indicate a clear east–west gradient with diminishing influence of Pacific SSTA with increasing distance from the coast.

While the influence of ENSO on the coastal lowlands of Ecuador has been well established for a long time, this study yields new evidence as to how the ENSO signal is modified in several ways in different parts of the Andes of Ecuador eventually leading to a complete reversal of the response in the eastern and northwestern part of the Andes. The transition from one extreme response to the other is complex and not uniform and depends on the region and the season analyzed. This study provides evidence for both Pacific and Atlantic influence in a comparatively small area based on a dense station network. Current similar research using a high density station network is under way in the Peru–Bolivian Andes, where conditions are very similar, featuring a wet El Niño signal on the Peruvian coast eventually changing into drought conditions up on the Peru–Bolivian Altiplano (Vuille 1999). Based on the presented results, further work will also involve more detailed synoptic climatological analyses to better understand the physical mechanisms behind the links between tropical SSTA and climate variability in the Andes.

REFERENCES

Aceituno, P., 1988: On the functioning of the Southern Oscillation in the South American sector. Part I: Surface climate. *Mon. Wea. Rev.,* **116,** 505–524.

Bendix, J., and W. Lauer, 1992: The rainy seasons in Ecuador and their climatic interpretation (in German). *Erdkunde,* **46,** 118–134.

Chu, P.-S., Z.-P. Yu, and S. Hastenrath, 1994: Detecting climate change concurrent with deforestation in the Amazon basin: Which way has it gone? *Bull. Amer. Meteor. Soc.,* **75,** 579–583.

Chung, J. C., 1982: Correlations between the tropical Atlantic trade winds and precipitation in northeastern Brazil. *J. Climatol.,* **2,** 35–46.

Davis, R. E., 1976: Predictability of sea surface temperature and sea level pressure anomalies over the North Pacific Ocean. *J. Phys. Oceanogr.,* **6,** 249–266.

Enfield, D. B., and D. A. Mayer, 1997: Tropical Atlantic SST variability and its relation to El Niño–Southern Oscillation. *J. Geophys. Res.,* **102,** 929–945.

Goldberg, R. A., G. Tisnado, and R. A. Scofield, 1987: Characteristics of extreme rainfall events in Northwestern Peru during the 1982–1983 El Niño period. *J. Geophys. Res.,* **92** (C13), 14 225–14 241.

Halpert, M. S., and C. F. Ropelewski, 1992: Surface temperature patterns associated with the Southern Oscillation. *J. Climate,* **5,** 577–593.

Hameed, S., K. R. Sperber, and A. Meinster, 1993: Teleconnections of the Southern Oscillation in the tropical Atlantic sector in the OSU coupled upper ocean–atmosphere GCM. *J. Climate,* **6,** 487–498.

Hastenrath, S., 1981: *The Glaciation of the Ecuadorian Andes.* Balkema, 173 pp.

——, 1990: Diagnostics and prediction of anomalous river discharge in northern South America. *J. Climate,* **3,** 1080–1096.

——, and L. Heller, 1977: Dynamics of climatic hazards in northeast Brazil. *Quart. J. Roy. Meteor. Soc.,* **103,** 77–92.

Horel, J. D., and A. G. Cornejo-Garrido, 1986: Convection along the coast of northern Peru during 1983: Spatial and temporal variation of clouds and rainfall. *Mon. Wea. Rev.,* **114,** 2091–2105.

Karl, T. R., A. J. Koscielny, and H. F. Diaz, 1982: Potential errors in the application of principal component (eigenvector) analysis to geophysical data. *J. Appl. Meteor.,* **21,** 1183–1186.

Kayano, M. T., V. B. Rao, and A. D. Moura, 1988: Tropical circulation and the associated rainfall anomalies during two contrasting years. *J. Climatol.,* **8,** 477–488.

Kousky, V. E., and M. T. Kayano, 1994: Principal modes of outgoing longwave radiation and 250-mb circulation for the South American sector. *J. Climate,* **7,** 1131–1143.

Liebmann, B., and C. A. Smith, 1996: Description of a complete (interpolated) outgoing longwave radiation dataset. *Bull. Amer. Meteor. Soc.,* **77,** 1275–1277.

Marengo, J. A., 1992: Interannual variability of surface climate in the Amazon basin. *Int. J. Climatol.,* **12,** 853–863.

——, and S. Hastenrath, 1993: Case studies of extreme climatic events in the Amazon basin. *J. Climate,* **6,** 617–627.

Mechoso, C. R., S. W. Lyons, and J. A. Spahr, 1990: The impact of sea surface temperature anomalies on the rainfall over northeast Brazil. *J. Climate,* **3,** 812–826.

Nobre, P., and J. Shukla, 1996: Variations of sea surface temperature, wind stress, and rainfall over the tropical Atlantic and South America. *J. Climate,* **9,** 2464–2479.

North, G. R., T. L. Bell, R. F. Cahalan, and F. J. Moeng, 1982: Sampling errors in the estimation of empirical orthogonal functions. *Mon. Wea. Rev.,* **110,** 699–706.

Overland, J. E., and R. W. Preisendorfer, 1982: A significance test for principal components applied to a cyclone climatology. *Mon. Wea. Rev.,* **110,** 1–4.

Poveda, G., and O. J. Mesa, 1997: Feedbacks between hydrological processes in tropical South America and large-scale ocean–atmospheric phenomena. *J. Climate,* **10,** 2690–2702.

Rasmusson, E. M., and T. H. Carpenter, 1982: Variations in tropical sea surface temperature and surface wind fields associated with the Southern Oscillation/El Niño. *Mon. Wea. Rev.,* **110,** 354–384.

Richman, M. B., and P. J. Lamb, 1985: Climatic pattern analysis of three- and seven-day summer rainfall in the central United States: Some methodological considerations and a regionalization. *J. Climate Appl. Meteor.,* **24,** 1325–1343.

Rossel, F., 1997: *Influence of El Niño on the hydrological regime of Ecuador* (in Spanish). Serie INSEQ, Vol. 18, Republica del Ecuador, Ministerio de Energia y Minas, INAMHI, ORSTOM, 203 pp.

Servain, J., 1991: Simple climatic indices for the tropical Atlantic Ocean and some applications. *J. Geophys. Res.,* **96,** (C8), 15 137–15 146.

Stearns, S. D., and R. A. David, 1988: *Signal processing algorithms.* Prentice-Hall Signal Processing Series, Prentice-Hall, 349 pp.

Tapley, T. D., and P. R. Waylen, 1990: Spatial variability of annual precipitation and ENSO events in western Peru. *Hydrol. Sci. J.,* **35,** 429–446.

Uvo, C. B., C. A. Repelli, S. E. Zebiak, and Y. Kushnir, 1998: The relationships between tropical Pacific and Atlantic SST and northeast Brazil monthly precipitation. *J. Climate,* **11,** 551–562.

Venegas, S. A., L. A. Mysak, and D. N. Straub, 1996: Evidence for interannual and interdecadal climate variability in the South Atlantic. *Geophys. Res. Lett.,* **23** (19), 2673–2676.

Vuille, M., 1999: Atmospheric circulation over the Bolivian Altiplano during DRY and WET periods and extreme phases of the Southern Oscillation. *Int. J. Climatol.,* **19,** 1579–1600.

——, R. S. Bradley, and F. Keimig, 2000: Interannual climate variability in the Central Andes and its relation to tropical Pacific and Atlantic forcing. *J. Geophys. Res.,* in press.

Wagner, R. G., 1996: Mechanisms controlling variability of the interhemispheric sea surface temperature gradient in the tropical Atlantic. *J. Climate,* **9,** 2010–2019.